Monte Carlo simulations on thermodynamic and conformational properties of catenated double-ring copolymers

Dachuan Sun and Junhan Cho*

Department of Polymer Science and Engineering, and Center for Photofunctional Energy Materials, Dankook University, 152 Jukjeon-ro, Suji-gu, Yongin, Gyeonggi-do 448-701, South Korea

(Received 2 June 2014; published 1 December 2014)

The thermodynamic and conformational properties of catenated double-ring A-B copolymer melts are investigated through lattice Monte Carlo simulations. The topological constraint on the catenated copolymers is shown to suppress demixing of A and B monomers. This action results in their order-to-disorder transition (ODT) at an increased segregation level and the lamellae below ODT with reduced order, when compared to diblock copolymers of linear or single-ring topology. The A and B rings are pulled closer by catenation in the copolymer, which leads to its smaller gyration radius, lamellar domain spacing, and distance between mass centers of the two rings than for the diblock copolymers. With increasing segregation tendencies, the gyration radii of the A rings of the catenated copolymers stretch along the direction normal to lamellae, while the A-block conformations of the single-ring copolymers change their shapes from ellipsoid to sphere.

DOI: 10.1103/PhysRevE.90.062601 PACS number(s): 61.25.hk, 64.75.Gh, 64.75.Yz

I. INTRODUCTION

Owing to the absence of free chain ends, ring polymers have higher glass transition temperatures, lower melting temperatures, and viscosity than their linear counterparts [1–5]. Recently, the ring copolymers with a θ shape [6], 8 shape [7,8], and tadpole shape [9] have been synthesized by a combination of living polymerization and click chemistry. Two single-rings can be catenated together to form a double-ring topology, which has also been synthesized recently [10–12]. Rather than chemical bonds, the two rings of the double-ring polymers are locked by topological constraints. Depending on the monomer sequences, the ring polymers can be homopolymers or copolymers [13,14]. Double-ring copolymers [as shown in Fig. 1(a)] are formed by two catenated homopolymer rings, and the whole chain contains two kinds of monomers. The dynamic, thermodynamic, and conformational properties of the catenated double-ring polymers are expected to be different from those of the linear or single-ring polymers [15,16].

As the double-ring polymers are difficult to synthesize and purify, one method to investigate their physical properties is the Monte Carlo (MC) simulation. The MC method can avoid the formation of knottiness within each ring and maintain the topological constraints between the two rings, which is difficult to handle in other theoretical or simulation methods [17,18]. Previous relevant MC simulations have dealt with the double-ring homopolymers with two rings formed by the same monomers. Otto [19] investigated the free energy for a pair of linked homopolymer rings with distance R between two segments of different rings and found that the effective topological interaction scales as R^4. MC simulations by Pakula [20] dealt with the elasticity and dynamics of catenated homopolymers. Catenanes were found to be in general more compact than the linear or cyclic chains with the same total length.

So far, there have been few investigations into the molecular physics of catenated double-ring copolymers, in which each ring is composed of a single component. It is then the objective of this work to use the MC simulations to investigate the thermodynamic and conformational properties of such catenated double-ring copolymers, with a focus on the order-to-disorder transition (ODT) values, and the changes in domain sizes and copolymer conformations with temperature. The resultant properties of the double-ring copolymers are compared to those of the diblock copolymers of linear or single-ring topology having the same total chain length to elucidate the effect of topological constraint on their behaviors.

II. MODEL AND SIMULATION METHODS

Lattice Monte Carlo simulations are carried out in a cubic box with a size of $L_x \times L_y \times L_z = 60^3$, where L_J is given in terms of a lattice unit-cell edge length σ. Periodic boundary conditions are imposed on all three directions. Here we consider only the melts of symmetric AB copolymers with composition $f_A = 0.5$. To accelerate the relaxation of chain conformations, 11.1% permanent vacancies (denoted as V) are allowed in the simulation box. Permanent vacancies can be deemed neutral solvents or free spaces. Figure 1 shows our target material of the catenated double-ring A-B copolymer along with the AB diblock copolymers of linear and ring architectures. All three types of copolymers are chosen to possess the same total length N of 40, where N is the sum of individual sizes of the two rings for the catenated double rings. For convenience, the linear, single ring. and catenated double rings are denoted as L, S, and D, respectively. The artifacts caused by the periodic boundary can be avoided, as the simulation box size is more than 10 times the radius of gyration of copolymers and the ordered lamellae have at least three periodic layers. The bond length varies from 1σ to $\sqrt{2}\sigma$. Each segment occupies one lattice site and obeys the excluded volume criterion. To maintain the topological constraint between the two catenated rings and to avoid the formation of knottiness within each ring, the bond crossing is always forbidden during the relaxation and after each movement.

*jhcho@dankook.ac.kr

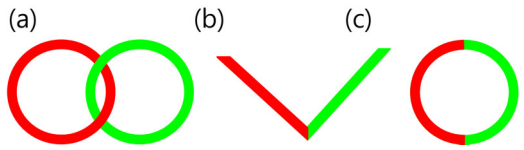

FIG. 1. (Color online) Schematic plots for (a) catenated double-ring A-B copolymers along with AB diblock copolymer of (b) linear and (c) single-ring topologies. Red (or black) and green (or gray) colors represent A and B monomers, respectively. All copolymers have the same total length N.

In the present work, we consider only the pairwise nearest-neighbor interactions. For further simplicity, only the interaction between A and B segments, which is denoted as $\varepsilon_{\mathrm{AB}}$, is taken into account, while all other interactions are set to be zero. Thus, the system possesses $\varepsilon_{\mathrm{AB}} > 0$ (repulsive) and $\varepsilon_{\mathrm{AA}} = \varepsilon_{\mathrm{BB}} = \varepsilon_{\mathrm{VV}} = \varepsilon_{\mathrm{AV}} = \varepsilon_{\mathrm{BV}} = 0$. All simulations are started by equilibrating the systems in the athermal limit, i.e., $\varepsilon_{AB}/k_BT = 0$, where k_{B} denotes the Boltzmann constant and T is temperature. Then those totally disordered configurations are quenched to any required values of ε_{AB}/k_BT, and the system is to be equilibrated again.

The evolution of chain configuration is achieved by vacancy diffusion algorithm, wherein vacancy sites are selected first and to be exchanged with a neighbor polymer segment. The movement style called partial reptation [21,22] is included to accelerate the simulation process. One Monte Carlo step (MCS) is defined as the time necessary for every segment to attempt to move once on average. Every attempted move should obey the excluded volume criterion, the bond length restriction, and no bond-crossing criterion, which is further judged by the Metropolis scheme [23]. The Boltzmann factor, $\exp(-\Delta E/k_{\mathrm{B}}T)$, should be greater than or equal to a random number uniformly distributed in the interval (0,1), where ΔE is the change in energy due to this attempted move. During the simulation, we monitor the evolution of the average energy per monomer [24] (E_{m}) and the structural properties [such as the structure factor $S(q)$] of the system. The equilibration is considered to be reached when those quantities do not change with the simulation time. Starting from totally disordered states, generally at least 10^7 MCSs are required to equilibrate the system, and another 10^7 MCSs are used to collect the data.

In MC simulations, every detail of the resultant microstructures can be examined [25]. The effective Flory-Huggins interaction parameter χ is calculated as follows using the method proposed by Pakula [24]:

$$\chi = \frac{\langle E_m \rangle}{2k_BT\varphi_A\varphi_B} \tag{1}$$

where $\langle E_m \rangle$ implies the thermally averaged energy. The volume fractions ϕ_j for A and B monomers are the same as $\phi_A = \phi_B = 0.444$. The structure factor [24] is calculated as

$$S(q) = \frac{1}{mN}\sum_i\sum_j e^{i\vec{q}\cdot(\vec{r}_i-\vec{r}_j)}\langle c_k(\vec{r}_i)c_l(\vec{r}_j)\rangle \tag{2}$$

where $\vec{q}$ is the scattering vector and m indicates the number of copolymer chains. The symbols c_k and c_l denote the contrast operators, which take values 1 or -1 if the monomer at a given local position $\vec{r}_i$ is A or B, respectively.

The phase domain size D is obtained from the reverse of characteristic wave vector $q_{\max}$ as

$$D = 2\pi/q_{\max} \tag{3}$$

where $S(q)$ exhibits its primary peak at $q_{\max}$. To acquire the conformational information of copolymer chains, the radius of gyration [26] is calculated as

$$R_{\mathrm{g}} = \left[\frac{1}{mN}\sum_{i=1}^{m}\sum_{j=1}^{N}\left(r_j^i - R_{\mathrm{C.M.}}^i\right)^2\right]^{1/2} \tag{4}$$

where $R_{\mathrm{C.M.}}^i$ indicates the position of the mass center of the ith copolymer chain. The symbol $\vec{r}_j^{\,i}$ denotes the coordinates of j monomer on the ith copolymer. To reflect the variations of copolymer conformations along the normal and parallel directions to the lamellar layer, the components of R_{g^2} including $R_{\mathrm{g_{xy}}}^2$ [$\equiv\frac{1}{2}(R_{\mathrm{g_x}}^2 + R_{\mathrm{g_y}}^2)$] and $R_{\mathrm{g_z}}^2$ are also measured, where R_{gx}^2 and R_{gy}^2 are those in plane parallel to the lamellar interface, and R_{gz}^2 is the remaining one. We determine the radii of gyration for the A and B rings or blocks, which are denoted as $R_{\mathrm{g,A}}$ and $R_{\mathrm{g,B}}$, respectively. There are two additionally important lengths, which are the distance d_{M} between the mass centers of the A and B rings or blocks, and the distance d_{J} between the junction points of the single ring copolymer. These quantities are all measured in terms of the lattice constant σ.

To get the averaged value of data and estimate the error bar, five independent simulations starting from totally random initial configurations are relaxed for the same time, i.e., 10^7 MCS. Then the static and thermodynamic properties are extracted from the final equilibrated states. During the simulations, the normal direction to lamellae formed by each kind of diblock copolymers is not exactly along the axis direction. Instead, it can be automatically adjusted during the self-assembly process. Thus, except for very high segregation strengths, the lamellae developed through the self-assembly of the given copolymers are considered to possess the optimum layer-layer separations. For a box of $L_J = 60$, the lamellar morphology usually has more than four periodic layers, and the constraint exerted by the periodic boundary condition should be small. We then repeated the calculation of $N\chi$ at different boxes with $L_J = 80$ and 100 (in cubic shape) for concatenated double-ring copolymers and found that the deviation in $N\chi$ is within 3%. The deviations in conformational properties turn out to be within 7%. These results suggest that our data obtained from a box with $L_J = 60$ can avoid artifacts from the periodic boundary condition.

III. RESULTS AND DISCUSSION

Let us now examine our MC results for the copolymers of our interest. It is a stringent test to compare effective $N\chi$ values at ODT from the simulations to theoretical ones. Hereafter T is taken for simplicity as k_BT/ε_{AB}. In Fig. 2, $N\chi$ from Eq. (1) is plotted against the dimensionless T. The positions of T_{ODT} for the three copolymers are determined when there appear the discontinuous changes in $N\chi$. The observed discontinuity in $N\chi$ indicates that the order-disorder transitions for these

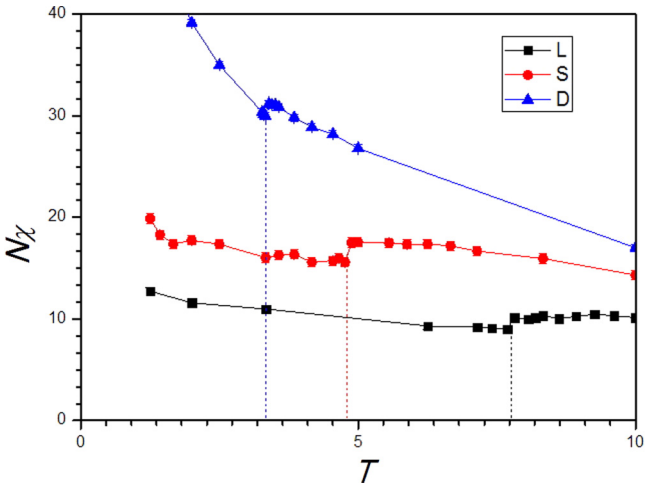

FIG. 2. (Color online) Effective $N\chi$ plotted against dimensionless temperature T for the copolymers with catenated double-ring (D), linear (L), and single-ring (S) architectures. Dotted lines indicate T_{ODT} for the three copolymers.

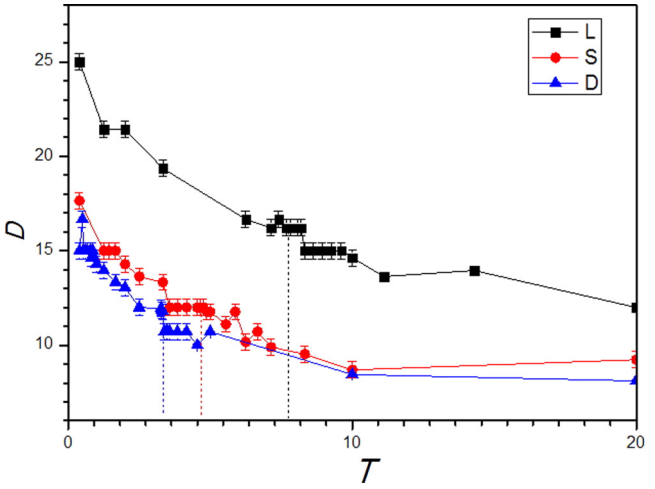

FIG. 3. (Color online) Domain size D plotted against temperature T for the copolymers with catenated double-ring (D), linear (L), and single-ring (S) architectures. Domain size D is given in terms of lattice constant σ.

three copolymers are all of first order. The copolymers at $T < T_{\mathrm{ODT}}$ assemble into the lamellar phase due to their symmetric compositions. The linear diblock copolymers are shown to have $(N\chi)_{\mathrm{ODT}} = 10.35$, which approaches the predicted value of 10.5 [27]. The single-ring copolymers in our MC simulations yield $(N\chi)_{\mathrm{ODT}} = 17.5$, which is slightly lower than the theoretical value of $(N\chi)_{\mathrm{ODT}} = 17.8$ given in previous self-consistent mean field calculations [28]. It should be noted that according to MC simulations by Brown *et al.* [29], the constraints preventing different bonds from passing through one another have strong influences on the structure and dynamics of rings at higher volume fractions. $(N\chi)_{\mathrm{ODT}}$ drops to 16.9 when bond crossing restrictions are turned off for single-ring copolymers. It is seen from Fig. 2 that the symmetric catenated double-ring copolymers are found to possess $(N\chi)_{\mathrm{ODT}} = 31.2$. It is then evident that the topological constraint on the catenated copolymers suppresses demixing of the dissimilar monomers to cause their ODT at the increased segregation strength.

The domain size of a microphase formed by copolymers is an important quantity, as copolymers can be used as scaffolds to produce nanomaterials or as templates to direct the self-assembly of nanoparticles. We compare in Fig. 3 the domain sizes of lamellar morphologies for the three copolymers. Previous experimental investigations indicate that ring block copolymers yield the lamellae of smaller domain sizes than the corresponding linear copolymers [30–32]. Our simulation results are consistent with this observation. Marko [33] theoretically investigated the microphase separation of single-ring copolymers without considering further topological constraints on them. According to Marko's calculation, the ratio $D_{\mathrm{S}}/D_{\mathrm{L}}$ of domain sizes between ring and linear diblock copolymer melts decreases from 0.67 to 0.63 with increasing segregation strengths. Jo *et al.* reported the ratio of $D_{\mathrm{S}}/D_{\mathrm{L}} = 0.70$ at ODT using the MC simulations [34]. Our simulations reveal that $D_{\mathrm{S}}/D_{\mathrm{L}}$ decreases from 0.78 to 0.50 with increasing segregation strengths, and $D_{\mathrm{S}}/D_{\mathrm{L}}$ at ODT is found to be 0.72, which is consistent with the simulations by Jo *et al.* Figure 3 also shows that $D_{\mathrm{D}}/D_{\mathrm{S}} = 0.94$ and $D_{\mathrm{D}}/D_{\mathrm{L}} = 0.69$ at their respective ODTs. It is shown in this figure that at the same temperature, the domain sizes of the lamellae for the catenated double-ring copolymers are smaller than those for the linear or single-ring copolymers of the same length.

In the double-ring copolymers, a portion of monomers are involved in sustaining the topological constraints. Thus, fewer monomers are used for changing the chain conformations than in the copolymers of other architectures. This action reduces the stretched length of copolymers along the direction normal to lamellae and decreases the lamellar domain size. Our simulations reveal that the catenated diblock copolymers possess the smallest domain size among those three copolymer structures. Ohta *et al.* suggested in their experiments that the domain size of double-ring copolymers is between those of the linear and single-ring copolymers of the same lengths [35].

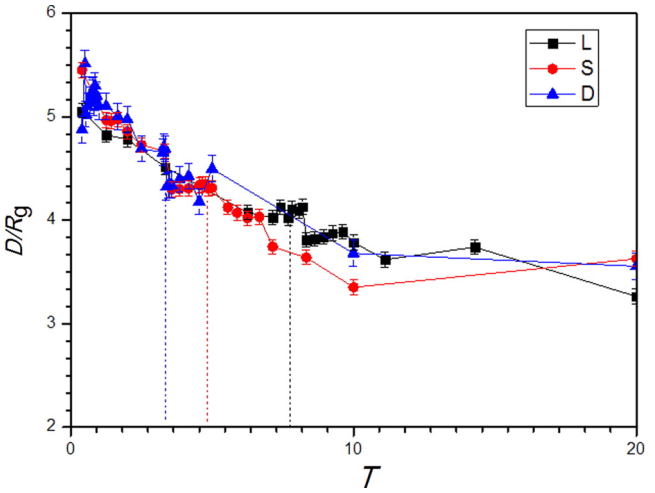

FIG. 4. (Color online) Ratio of domain size D to gyration radius R_{g} plotted against temperature T for the copolymers with catenated double-ring (D), linear (L), and single-ring (S) architectures. The gyration radius R_{g} is again given in terms of σ.

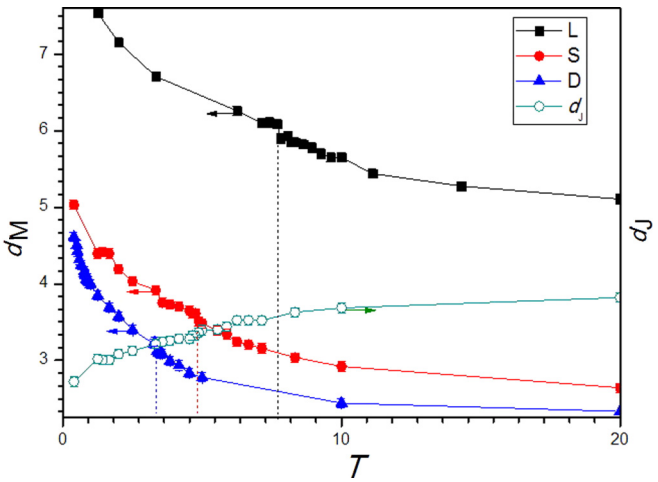

FIG. 5. (Color online) Distance d_M between the mass centers of the A and B rings or blocks as a function of temperature T for the copolymers with the double-ring (filled triangles), linear (filled squares), and single-ring (filled circles) architectures. The distance d_J between the two junction points of the single ring copolymer (empty circles) are drawn together. Distances d_M and d_J are again given in terms of σ.

However, their measurements were done at strong segregation strengths on the double-ring copolymers of high molecular weights. For a sufficiently long double-ring copolymer chain, only a small fraction of monomers are wasted to sustain the catenated constraint. In this case, the elongation of the double-ring chain can be viewed as two doubly folded chains with a single hooking (physical junction) point. In contrast, a single-ring copolymer chain under elongation can be regarded as a doubly folded chain with two chemical junction points. Therefore, double-ring copolymers can be less resistant to stretching than single-ring copolymers. This procedure may lead to a larger lamellar domain size for the former than the latter. Such a notion seems plausible for long copolymer chains or alternatively at strong enough segregation strengths, which is currently not observed in our simulations.

From the enthalpic viewpoints, stretching copolymer chain conformations away from interface is helpful to weaken unfavorable A-B contacts. For athermal polymer chains, Zimm *et al.* [36] found that the ratio R_{gS}^2/R_{gL}^2 of gyration radii between single-ring and linear copolymers is estimated to be 0.5. However, the excluded volume effect was neglected in their calculations. It was shown by Qian *et al.* [37] using dissipative

TABLE I. Components of gyration radius R_g for a whole copolymer molecule and gyration radius $R_{g,A}$ for A ring/block along the x, y, and z axes in cases of double-ring (D) and single-ring (S) copolymers.

Topology	T	R_g	$R_{g_{xy}}$	R_{g_z}	$R_{g,A}$	$R_{g,A,xy}$	$R_{g,A,z}$
D	3.33	2.54	1.29	1.64	1.93	1.09	1.14
D	1.67	2.69	1.23	2.05	1.94	1.06	1.22
S	3.33	2.85	1.48	2.01	2.08	1.22	1.16
S	1.67	3.02	1.39	2.32	2.07	1.19	1.16

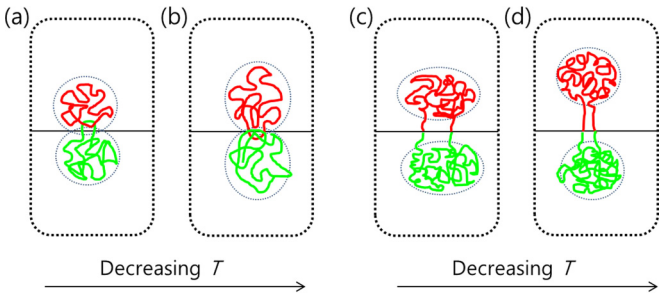

FIG. 6. (Color online) Schematic cartoons for the chain conformations of double-ring copolymers at (a) a lower and at (b) a higher segregation strength. The dotted circles depict the conformational clouds formed by A and B rings. The cartoons in (c) and (d) show the changes in the copolymer conformations of single-ring copolymers with increasing segregation strengths.

particle dynamics (DPD) simulations that $R_{gS}^2/R_{gL}^2 = 0.463$ at their respective ODTs. Our simulations under both the bond crossing and excluded volume criteria indicate that the ratio $R_{gS}^2/R_{gL}^2 = 0.468$, which is consistent with the work of Qian *et al.* In the athermal state, $R_{gS}^2/R_{gL}^2 = 0.484$ under the excluded volume criterion, which is slightly smaller than the predicted value 0.5 without considering the excluded volume effect. The ratio R_{gD}^2/R_{gS}^2 between double-ring and single-ring copolymers increases with the segregation strength. The R_{gD}^2/R_{gS}^2 changes from 0.77 to 0.90 at temperature T from 10 to 1.

Figure 4 shows the ratio of the lamellar domain size D to the gyration radius R_g for the copolymers at different temperatures. This ratio is considered to reflect the amplitude of mutual diffusion of copolymer conformations along the normal direction to lamellar layers. It is seen in this figure that D/R_g is not influenced by the topology of copolymers. The

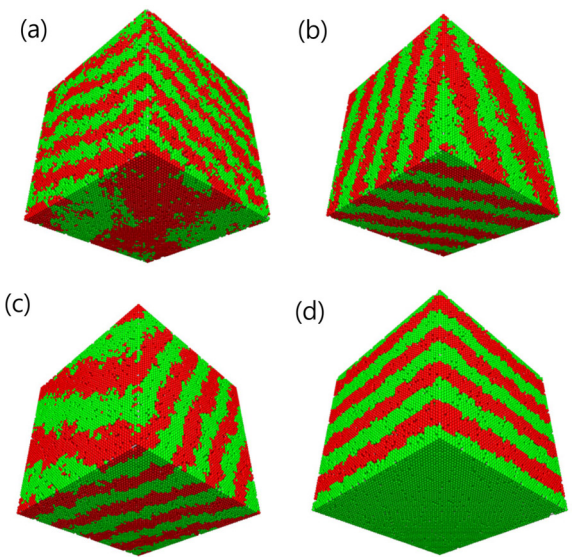

FIG. 7. (Color online) Snapshots of lamellae for double-ring copolymer melts at (a) $T = 3.33$ and (b) $T = 1.67$. Those marked by (c) and (d) visualize the lamellae of single-ring copolymers at $T = 3.33$ and $T = 1.67$, respectively.

increase of D/R_g with the segregation tendencies (decreasing T) implies the diminished mutual diffusion. The ratio D/R_g for linear diblock copolymers is near 4 at ODT. At $T < T_{ODT}$, D/R_g becomes larger than 4.0, which indicates the highly stretched copolymer conformations and/or the reduced mutual diffusion of copolymer conformations between the neighboring lamellar layers.

It is shown in Fig. 5 that the distance parameter d_M for all three copolymers increases with the segregation strength. The ratio of d_M values between the linear and single-ring structures is calculated to be 1.9 from our MC simulations, and 1.8 by Qian *et al.* using the DPD simulation method [37]. With increasing segregation strengths, d_M for double-ring copolymers approaches but is still lower than that for single-ring copolymers. Thus, the topological constraint on the double-ring copolymers pulls the A and B rings closer, which results in the smallest d_M, R_g, and D values among the three copolymers. In case of single-ring copolymers, the interjunction distance d_J is found to be decreased towards zero with the segregation strength. The conformations of the ring copolymers thus stretch in the normal direction to lamellar interface and shrink along the interface. Deduced from this observation, the shape of the single-ring copolymer may maintain a dumbbell morphology, and its higher R_g at lower temperatures may mainly arise from the enlarged distance d_M between the mass centers of the A and B blocks.

The components of the gyration radius R_g for the whole double-ring copolymer chain and $R_{g,A}$ for the A ring only at two selected temperatures below ODT are tabulated in Table I. The z axis is chosen to be the direction normal to lamellae, and thus x and y imply the remaining two parallel directions. With increasing segregation strengths, the conformation of a whole copolymer chain as well as that of the A ring only stretch along the normal direction. It is seen from Table I that the ratios $R_{g_z}/R_{g_{xy}}$ and $R_{g,A,z}/R_{g,A,xy}$ become larger at the lower temperature. A schematic plot is given in Figs. 6(a) and 6(b) to show this change in chain conformations of the double-ring copolymers, and the snapshots representing these two samples are given in Figs. 7(a) and 7(b), respectively. According to the snapshots, there are many B monomers distributed within the A lamellar layers near the interface. These contacts between dissimilar monomers are enthalpically

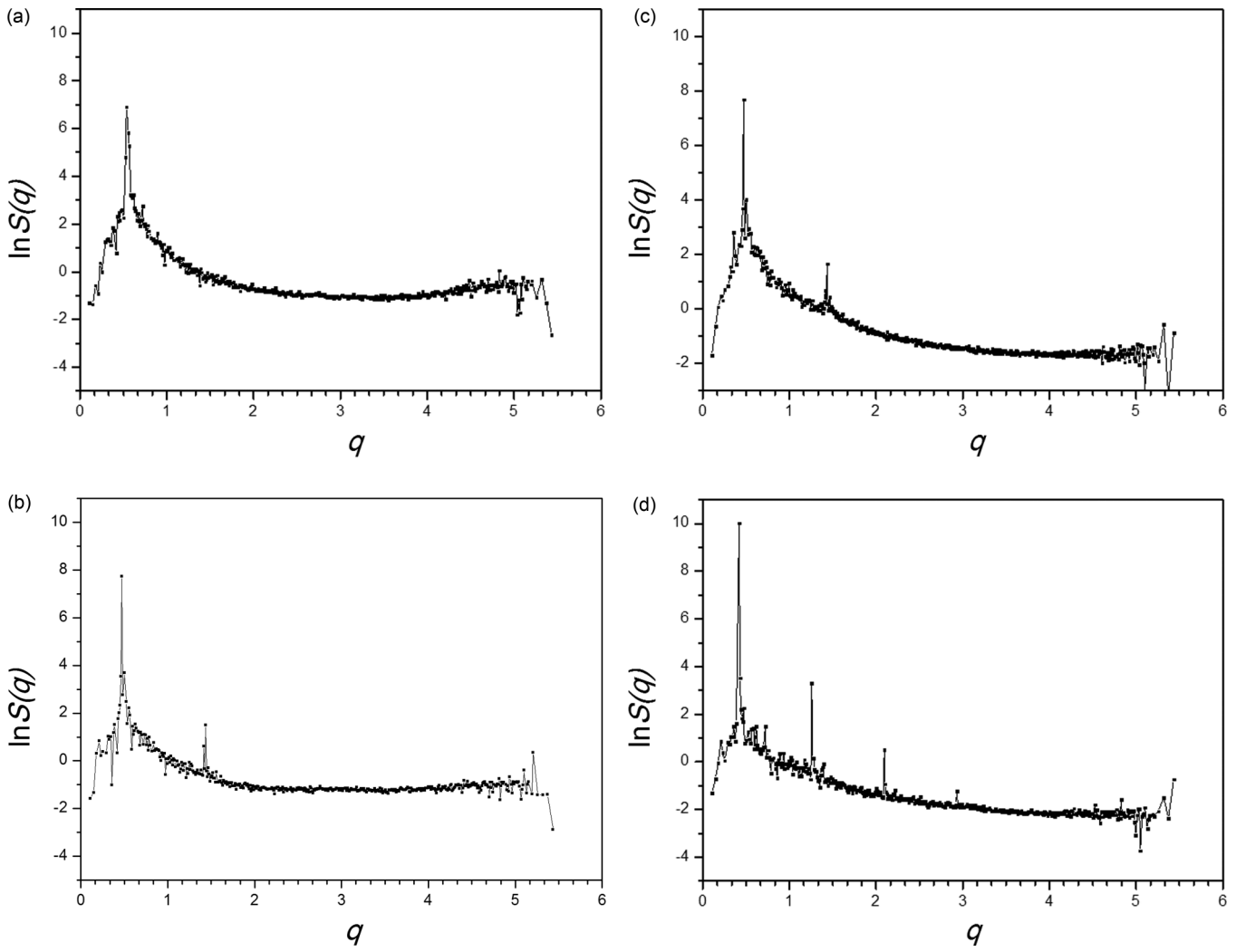

FIG. 8. Structure factors plotted against dimensionless scattering vector q, which is given in terms of $1/\sigma$, for the lamellae of double-ring copolymer melts at (a) $T = 3.33$ and (b) $T = 1.67$. Those marked by (c) and (d) stand for single-ring copolymers at $T = 3.33$ and $T = 1.67$, respectively.

unfavorable but are fixed by topological constraint on the catenated copolymers. In case of single-ring copolymers, the normal component of $R_{g,A}$ for the A block is smaller than its two parallel components, which is in contrast to the components of R_g for the whole chain. Figures 6(c) and 6(d) schematically depict such an alteration of chain conformations in the lamellae with the segregation strength. Statistically, the conformations of the A blocks, and B also, can be viewed as clouds. The whole copolymer possesses a dumbbell shape, but the conformational clouds formed by the A blocks deviate from the spherical shape. Such a deviation fades out at higher segregation strengths. The corresponding morphological snapshots are given in Figs. 7(c) and 7(d), respectively.

Figure 8 displays the structure factors for the four samples in Fig. 7. There appear no higher-order peaks for the double-ring copolymers in Fig. 8(a), because its temperature is close to ODT, and the compositional fluctuations are augmented due to the topological constraint of catenation. In case of the single-ring copolymers at the same temperature, a higher-order peak is clearly seen in Fig. 8(c), because the topological constraint is absent and the developed lamellae are well ordered. As temperature is lowered, segregation is more developed. The scattering peaks with q ratio of 1:3 then appear in Fig. 8(b) for the double-ring copolymers. At the same temperature as in Fig. 8(b), the scattering factor given in Fig. 8(d) for the single-ring copolymer reveals more higher-order peaks signified by the peaks with q ratio of 1:3:5:7.

IV. CONCLUSIONS

We perform here lattice Monte Carlo simulations on catenated double-ring A-B copolymers to investigate into their thermodynamic and conformational properties. The topological constraint on the double-ring copolymers suppresses demixing of A and B monomers and pulls the two rings closer. The ODT for symmetric double-ring copolymers is first-order. The effective $N\chi$ at ODT for the double-ring copolymers is calculated to be 31.2, which is much higher than that for linear or single-ring diblock copolymers of the same chain length. Snapshots and structure factors indicate that the lamellae formed by the catenated copolymers are less ordered than those by the single-ring copolymers. Compared to the linear and single-ring diblock copolymers, the catenated copolymers reveal the smaller domain sizes, radii of gyration, and distances between the mass centers of A and B rings. With increasing segregation strengths, the A or B rings of the catenated copolymers stretch along the direction normal to lamellae, while the conformations of the A or B blocks of the single-ring copolymers change their shapes from ellipsoid to sphere.

ACKNOWLEDGMENTS

This work was supported by the Basic Science Research Program (No. 2014023297) from the National Research Foundation of Korea. The authors also acknowledge the support from the Center for Photofunctional Energy Materials, which is funded by Gyeonggi Regional Research Center Program (GRRCdankook2014-B03).

[1] C. W. Bielawski, D. Benitez, and R. H. Grubbs, Science **297**, 2041 (2002).
[2] M. Rubinstein, Phys. Rev. Lett. **57**, 3023 (1986).
[3] H. Takeshita, M. Poovarodom, T. Kiya, F. Arai, K. Takenaka, M. Miya, and T. Shiomi, Polymer **53**, 5375 (2012).
[4] J. Roovers, Macromolecules **18**, 1359 (1985).
[5] D. J. Orrah, J. A. Semlyen, and S. B. Ross-Murphy, Polymer **29**, 1452 (1988).
[6] G.-Y. Shi and C.-Y. Pan, Poly. Sci. A **47**, 2620 (2009).
[7] G.-Y. Shi and C.-Y. Pan, Macromol. Rapid Commun. **29**, 1672 (2008).
[8] G.-Y. Shi, J.-T. Sun, and C.-Y. Pan, Macromol. Chem. Phys. **212**, 1305 (2011).
[9] X. Wan, T. Liu, and S. Liu, Biomacromolecules **12**, 1146 (2011).
[10] Y. Gan, D. Dong, and T. E. Hogen-Esch, Macromolecules **35**, 6799 (2002).
[11] K. Ishikawa, T. Yamamoto, M. Asakawa, and Y. Tezuka, Macromolecules **43**, 168 (2010).
[12] A. K. Bunha, J. Mangadlao, M. J. Felipe, K. Pangilinan, and R. Advincula, Macromol. Rapid Commun. **33**, 1214 (2012).
[13] C. A. Schalley, K. Beizai, and F. Vögtle, Acc. Chem. Res. **34**, 465 (2001).
[14] Z. Niu and H. W. Gibson, Chem. Rev. **109**, 6024 (2009).
[15] S. T. Milner and J. D. Newhall, Phys. Rev. Lett. **105**, 208302 (2010).
[16] S. Y. Reigh and D. Y. Yoon, ACS Macro Lett. **2**, 296 (2013).
[17] C. R. A. Abreu and F. A. Escobedo, Macromolecules **38**, 8532 (2005).
[18] M. Bohn and D. W. Heermann, J. Chem. Phys. **132**, 044904 (2010).
[19] M. Otto, J. Phys. A **37**, 2881 (2004).
[20] T. Pakula and K. Jeszka, Macromolecules **32**, 6821 (1999).
[21] S. Ji and J. Ding, Langmuir **22**, 553 (2006).
[22] Z. Yang, Z. Pan, L. Zhang, and H. Liang, Polymer **51**, 2795 (2010).
[23] N. Metropolis, A. W. Rosenbluth, M. N. Rosenbluth, A. H. Teller, and E. Teller, J. Chem. Phys. **21**, 1087 (1953).
[24] T. Pakula and K. Matyjaszewski, Macromol. Theory Simul. **5**, 987 (1996).
[25] R. G. Larson, J. Chem. Phys. **91**, 2479 (1989).
[26] A. Weyersberg and T. A. Vilgis, Phys. Rev. E **48**, 377 (1993).
[27] L. Leibler, Macromolecules **13**, 1602 (1980).
[28] J. U. Kim, Y.-B. Yang, and W. B. Lee, Macromolecules **45**, 3263 (2012).
[29] S. Brown, T. Lenczycki, and G. Szamel, Phys. Rev. E **63**, 052801 (2001).
[30] R. L. Lescanec, D. A. Hajduk, G. Y. Kim, Y. Gan, R. Yin, S. M. Gruner, T. E. Hogen-Esch, and E. L. Thomas, Macromolecules **28**, 3485 (1995).

[31] A. Takano, O. Kadoi, K. Hirahara, S. Kawahara, Y. Isono, J. Suzuki, and Y. Matsushita, Macromolecules **36**, 3045 (2003).
[32] Y. Zhu, S. Gido, H. Iatrou, N. Hadjichristidis, and J. W. Mays, Macromolecules **36**, 148 (2003).
[33] J. F. Marko, Macromolecules **26**, 1442 (1993).
[34] W. H. Jo and S. S. Jang, J. Chem. Phys. **111**, 1712 (1999).
[35] Y. Ohta, Y. Kushida, D. Kawaguchi, Y. Matsushita, and A. Takano, Macromolecules **41**, 3957 (2008).
[36] B. H. Zimm and W. H. Stockmayer, J. Chem. Phys. **17**, 1301 (1949).
[37] H.-J. Qian, Z.-Y. Lu, L.-J. Chen, Z.-S. Li, and C.-C. Sun, Macromolecules **38**, 1395 (2005).